Received October 24, 2017, accepted November 21, 2017, date of publication November 28, 2017,
date of current version March 12, 2018.

Digital Object Identifier 10.1109/ACCESS.2017.2778071

Energy-Efficient Wireless Transmissions for Battery-Less Vehicle Tire Pressure Monitoring System

QINMIAO KANG[1,2], XUDONG HUANG[1], YONG LI[3], (Senior Member, IEEE), ZHIFENG XIE[1], YONGQUAN LIU[2], AND MING ZHOU[1]

[1]School of Aerospace Engineering, Tsinghua University, 100084 Beijing, China
[2]606 Institute, Chinese Aeronautical Establishment, 110015 Shenyang, China
[3]Department of Electronic Engineering, Tsinghua University, 100084 Beijing, China

Corresponding author: Zhifeng Xie (xzhf@tsinghua.edu.cn)

ABSTRACT This paper presents an energy-efficient wireless transmission scheme for battery-less vehicle tire pressure monitoring system (TPMS). Our proposed transmission scheme includes a wake-up communication link with 125-kHz carrier frequency and a data communication link with 433-MHz carrier frequency. Considering the TPMS application requirements and the special nature of the vehicle environment, we derive the relevant circuit parameters. In order to verify the reliability of the wireless communication system under the derived circuit parameters, we design an in-tire data transmitter and wake-up receiver. The 125-kHz wake-up receiver adopts dual-channel to improve the communication reliability and logarithmic amplifiers to achieve ASK demodulation and dynamic range compression. The receiver is implemented in 0.35-μm high voltage (HV) BCD process. Experiment results show that typical power consumption of the receiver is no more than 5 μA under 3.3 V supply voltage; the maximum data rate is 35 kb/s with 0.5 mVpp sensitivity. On the other hand, the data transmitter is implemented in 0.18-μm MMRF process. Experiment results show that the typical power consumption is 7.3 mA under 1.8 V supply voltage, and the emission power is -10 dBm@433.92 MHz with a phase noise of -103 dBc/Hz@300 kHz. System level experiments demonstrate that the proposed wireless transmission scheme fulfills the vehicle TPMS requirements. The data transmitter and wake-up receiver can communicate with the commercial data receiver and wake-up transmitter in the range of 20 m, which meets the requirements of most vehicles.

INDEX TERMS 125 kHz wake-up receiver, 433 MHz data transmitter, battery-less TPMS.

I. INTRODUCTION

With the development of automobile electronics, traffic safety has become an increasing demand, and Tire Pressure Monitoring System (TPMS) becomes an essential safety system in vehicles. US, SAE and ISO have issued the different TPMS standards [1]–[3], respectively. China also issued national recommended TPMS standard [4] in 2011. In general, TPMS products are powered by lithium batteries. Lithium battery has a limited life. As time goes by, the battery's performance will deteriorate; while replacing the lithium battery needs to disassemble the tire, which leads the operation very inconvenient. The drawback is that the deterioration of the battery performance has a bad impact on the precision and accuracy of TPMS. For the above-mentioned reasons, we propose a battery-less and energy-efficient TPMS scheme [5].

System architecture of the battery-less TPMS is shown in Fig.1. It is composed of tire status data processing module, display module and wireless communication module. The 13.56 MHz wireless energy transmission and power recovery module used to drive commercial TPMS products based on Infineon SP37, which is an off-the-shelf commercial chip and widely used in this area. It is an in-tire SoC which can process the tire status data, such as pressure and temperature, etc. Structure of the 13.56MHz wireless transmission and power recovery module is shown in Fig.2. Practical test environment of the wireless energy transmission and power recovery module is shown in Fig.3.

Due to the limited energy transmission capacity of the implemented wireless energy transmission module and its interference to TPMS wireless communication, battery-less

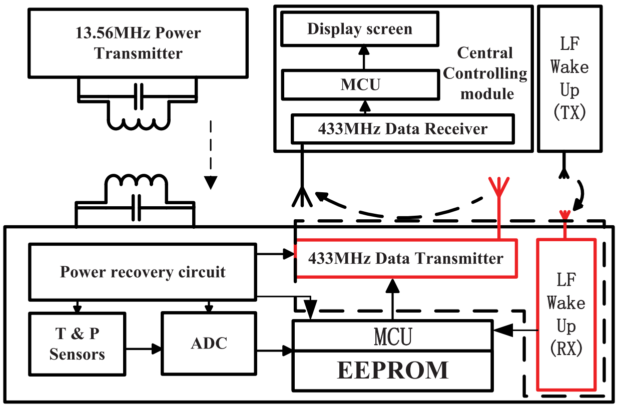

FIGURE 1. System architecture of the proposed battery-less TPMS.

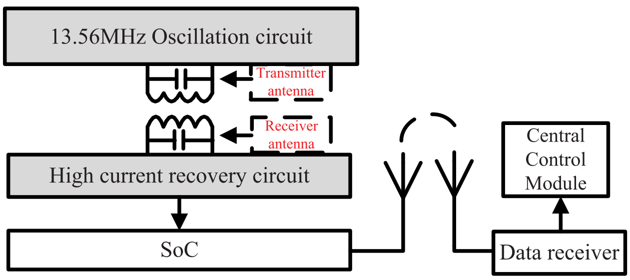

FIGURE 2. The 13.56 MHz wireless energy transmission and power recovery module.

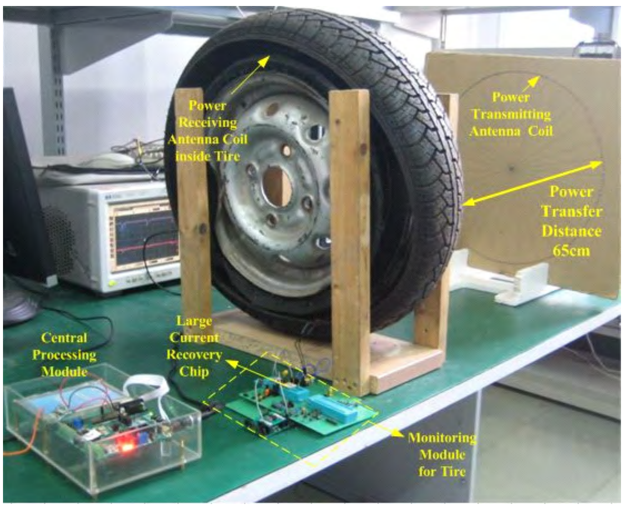

FIGURE 3. Practical test environment of the wireless energy transmission and power recovery module.

TPMS wireless communication module need to meet different requirements. These mainly includes low-power, data transfer reliability, anti-EMC and ESD protection ability and so on.

Wireless transmission is a key part in TPMS. The proposed wireless transmission scheme consists of two parts: the wake-up communication link for TPMS system low-power and the data communication link for the transmission and reception of tire status data, such as pressure, temperature, etc. Both of the above mentioned two communication links consist of a receiver and transmitter. To reduce the power consumption of the in-tire remote sensing module (RSM), a dual-band two-way communication scheme is adopted, in which the 433MHz communication link completes the transmission and reception of tire status data, and the 125kHz communication link for wake-up data. The proposed wireless communication scheme for battery-less TPMS is shown in Fig.4.

The rest of this paper is organized in the following way. In section II, derivation of the wireless transmission link for 125kHz wake-up communication link and 433MHz data transmission link are described in detail. It also gives a brief introduction to the wake-up receiver and data transmitter design parameters. In Section III and IV, we make a detail description on the 125kHz wake-up receiver and the 433MHz data transmitter's circuit design and chip test, respectively. In Section V, we conclude this paper and recommend directions for future research work.

II. DERIVATION OF WIRELESS TRANSMISSION LINK

In this section, we discuss the derivation of the transmission loss for 125kHz wake-up communication link and 433MHz data communication link. We will obtain the key design parameters of the transmitter and the wake-up receiver.

A. 125 kHz COMMUNICATION LINK CALCULATION

In the proposed TPMS wireless communication scheme, the 125kHz wake-up receiver needs to monitor the state of the wake-up signal all the time. Therefore, the receiver's low power design is very critical. According to the electromagnetic wave band division method, 125kHz belongs to the low frequency (LF); and according to its wavelength, it belongs to the long wave (LW) frequency band. Although 125kHz is out of the ISM frequency band, it can also be free to use since the frequency is below 135kHz.

Absorption rate of 125kHz for non-metallic materials and water is relatively low, and this frequency is much sensitive to the communication distance changes, thus it can be used in an inductive coupling way. The communication distance of LF is longer than that of the high-frequency (HF), but its data rate is low. The antenna transmission direction of the LF communication is not sensitive, so it has a stronger ability to bypass obstacles and better ability to anti-interference than that of HF communications [6].

LF wireless communication receivers are composed of frequency selection filters, amplifiers, demodulators, comparators and some other modules, the circuit design will be less difficult than that of the RF receiver. The basic transmission loss of electromagnetic waves [7] in free space can be found in:

$$L_{os} = 92.4478 + 20\lg D\,(m) + 20\lg f\,(MHz) \tag{1}$$

where L_{os} is transmission loss in the free space, with a unit dB; D is transmission distance, with a unit m; f is the frequency of electromagnetic waves, with a unit MHz.

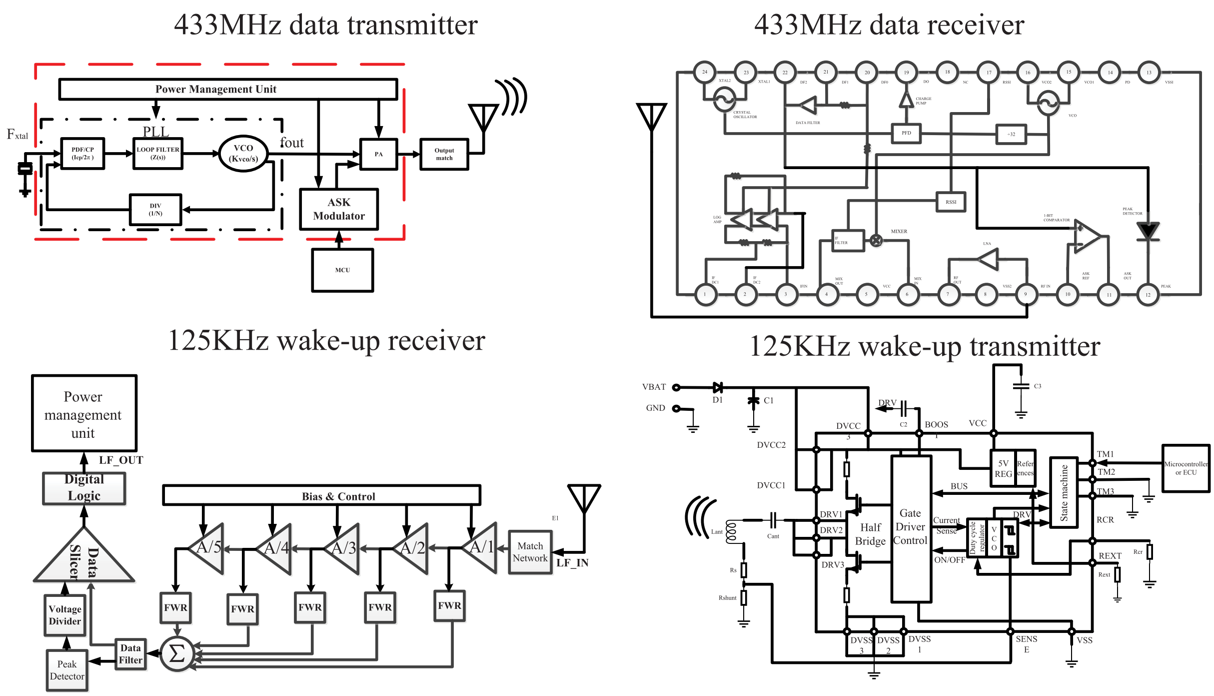

FIGURE 4. **The proposed wireless communication scheme for battery-less TPMS.**

The received power at the receiving end in the free space for the point-to-point transmission link [8] is:

$$P_r = P_t + G_t + G_r - L_t - L_r + L_{os} \tag{2}$$

where P_r is the received power in dBm; P_t is the transmitted power in dBm; G_t is the gain of the transmitting antenna in dBi; G_r is the gain of the receiving antenna in dBi; L_t is the transmitter intermediate loss in dB; L_r is the receiver intermediate loss in dB.

Setting $G_t = G_r = 2$dBi (usually 1-3dBi), D=20m, $L_t = L_r = 10$dB, $P_t = -10$dBm, f=0.125MHz in Eq.(1) and Eq.(2), we get $L_{os} = -16$dB, $P_r = -44$dBm. The conversion relationship between dBm and Vpp is:

$$\mathrm{dBm} = 20\lg\left(\mathrm{Vpp}/\sqrt{0.008 * Z}\right). \tag{3}$$

If the 50-ohm impedance matching is used, the Vpp value is about 5mVpp. Because this design works at low frequency, it is not necessary to consider the 50-ohm conjugate matching requirements, a higher resonant quality factor LC parallel resonant network can be selected to suppress noise and improve system sensitivity.

If the receiver sensitivity is too high, the noise signal and interference can easily flood the input signal, additional circuitry need to ensure the receiver demodulate correctly; it will increase the complexity of the circuit, therefore increase the overall system power consumption. Based on the above analysis, the receiver sensitivity is set to 4mVpp.

B. 433 MHz COMMUNICATION LINK CALCULATION

The communication quality of the wireless communication system is greatly influenced by the wireless channel; the wireless channel has a large randomness. The moving speed and temperature of the communication terminal also have a great influence on quality of the wireless communication [9]. In the 433MHz electromagnetic wave's transmission process, there are multipath loss, penetration and diffraction loss and other issues. When choose the transmission model, we need to take into account the above factors.

The wireless propagation model is divided into indoor model and outdoor model. The wireless communication of TPMS is suitable for outdoor model. The outdoor propagation model mainly includes Okumura model [10], Longley-Rice model [11] and Hata model [12]. According to the design of the application scenario, Okumura model is the most appropriate, it can be expressed by:

$$L_{50}(\mathrm{dB}) = L_f + A_{mu}(f, D) - G(h_t) - G(h_r) - G_{AREA} \tag{4}$$

where D is the distance between the transmitter and the receiver, L_{50} is 50% of the loss of the transmission path, L_f is the free space loss, $A_{mu}(f, D)$ is the median loss of free space, $G(h_t)$ is the antenna height gain factor of the transmitter, $G(h_r)$ is the antenna height gain factor of the receiver, G_{AREA} is the gain caused by the environment type. The values of A_{mu} and G_{AREA} can be obtained from the empirical values of the Okumura model [10]. And the empirical formula of $G(h_t)$ and $G(h_r)$ can be written as

$$G(h_t) = 20\lg(h_t/200), \quad 30\mathrm{m} < h_t < 1000\mathrm{m} \tag{5}$$

$$G(h_r) = \begin{cases} 10\lg(h_r/3) & h_r < 3\text{m} \\ 20\lg(h_r/3) & 3\text{m} < h_r < 10\text{m}. \end{cases} \quad (6)$$

The transmission loss is calculated according to the application environment of this design. The transmitter height changes as the wheel rotates; taking the mean and the transmitter is about at the center of the wheel, so the transmitter antenna height can be set as $h_t = 0.8$m. The receiver is placed in the central control module of the car cab, so we can assume that the receiver antenna height $h_r = 1$m. Taking into account the differences in the size of different vehicle types, assuming that the transmission distance D=20m, the free space transmission loss [13] can be calculated from

$$L_f = 10\lg\frac{G_l\lambda^2}{(4\pi D)^2} \quad (7)$$

where G_1 is the product of the transmitter and receiver antenna gain, and G_1=1 is assumed and λ is the wavelength of the carrier, thus we have

$$L_f = 10\lg\frac{(3*10^8/434*10^6)^2}{(4\pi*20)^2} = 51.2(\text{dB}). \quad (8)$$

By querying the Okumura model empirical-curve, we get

$$A_{mu}(f, D) = A_{mu}(434\text{MHz},20\text{m}) \approx 15\text{dB}. \quad (9)$$

Considering open areas, semi-open areas and suburbs and other correction factors and take the mean, we get

$$G_{AREA} \approx 18\text{dB}. \quad (10)$$

According to the actual situation of the vehicle, the 433MHz data transmitter antenna height is set to 0.8m, which does not meet the application conditions $30\text{m} < h_t < 1000\text{m}$ in Eq.(5). However, there are some reference value to use it to calculate the antenna height gain factor of the transmitter $G(h_t)$. From Eq.(5) and Eq.(6), we get

$$G(h_t) = 20\lg(0.8/200) \approx -48(\text{dB}) \quad (11)$$

$$G(h_r) = 10\lg(h_r/3) = 10\lg(1/3) \approx -4.8(\text{dB}). \quad (12)$$

Combining Eq.(4) and Eq.(8-12), we obtain

$$L_{50} = 51.2 + 15 - (-48) - (-4.8) - 18 = 101(\text{dB}). \quad (13)$$

Antenna effective omnidirectional transmit power (EIRP) is determined by

$$\text{EIRP (dBW)} = P_t\,(\text{dBW}) + G_t\,(\text{dBW})\,. \quad (14)$$

In general, 433MHz antenna gain is 2dBi, assuming that the transmitter's emission power $G_t = -10$dBm, one obtains the following from Eq.(14):

$$\text{EIRP}\,(dBW) = -8\text{dBW}. \quad (15)$$

Combining the Eq.(13) and Eq.(15), we get the received power

$$P_r\,(D) = \text{EIRP (dBW)} - L_{50}\,(\text{dB}) + G_r\,(\text{dBi}) = -107\text{dBm}. \quad (16)$$

According to the above derivation, the receiver sensitivity is −107dBm. Considering the influence of various non-ideal factors, the sensitivity of the receiver is determined to be −110dBm.

The 433MHz data transmitter transmits tire status data to the central control module in the cab. Design steps of 433MHz data transmitter are as follows: (1) According to the application requirements and related communication protocol, select the transmitter architecture, and determine the composition of the transmitter function module; (2) Simulate in system-level to get the design parameters; (3) Design the circuit to meet the parameters and verify the circuit; (4) Complete the layout design and design verification, includes ERC, DRC, LVS, PEX and post-layout simulation.

As the bit error rate of the transmitter is not high, but the power requirements are high, this design adopts ASK modulation. According to GB/T 26149-2010 provisions of high-frequency information frame length should not exceed 10ms, and a frame of this application is about 100bit. Taking into account the Ministry of Industry "micro power (short distance) radio equipment technical requirements" [13], the 433MHz data transmitter channel width is set to 300kHz, and the data rate is set to 20kbps.

According to GB/T 26149-2010 on the transmitter output power requirements, TPMS RF transmitter system should comply with the "Ministry of Information Industry Radio [2005] 423 micro-power (short distance) radio equipment technical requirements" for wireless control equipment requirements: When the tire pressure monitoring transmitter in 0-1 modulation state, the transmit power cannot exceed −20dBm. As TPMS wireless communication works intermittently, considering the proportion of time that the transmitter to send data to the total monitoring cycle, we can derive the maximum output power to meet the requirements is 2dBm. Therefore, the range of transmitter emission power is set to −15-2dBm.

Transmitter carrier signal is generated by the phase-locked loop (PLL). PLL phase noise will reduce the communication quality; considering the application requirements, the PLL phase noise is set −100dBc/Hz@300kHz, detailed PLL phase noise is derived in [14].

Since the transmitter normally operates in sleep mode, the tire pressure monitoring standard requires that the TPMS system monitors the tire pressure at regular intervals and require frequent opening and closing. If the PLL lock time is too long, the phase stabilization process will consume a large power, thus the PLL lock time is set to less than 150μs.

The transmitter adopts UMC 0.18μm MMRF 1P6M process, and the IO voltage is 3.3V (easy to connect with other tire monitoring module), the core voltage is 1.8V, the carrier frequency is 433.92MHz (UHF ISM). According to GB/T 26149-2010 requirements for in-tire monitoring module, Section E of the ETSI 300 220-1 V2.3.1 protocol [15] and Section 15.231 and Section 15.240 [16] of the US FCC

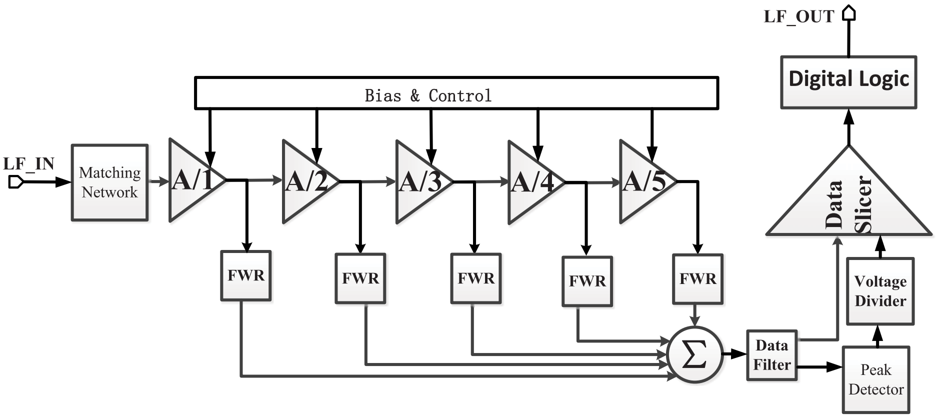

FIGURE 5. Architecture of 125 kHz LF wake-up receiver.

TABLE 1. 433MHz data transmitter design parameters.

Parameter	433MHz Data Transmitter
Supply Voltage(V)	1.8V (typical)
Carrier Frequency	433.92MHz
Temperature Range	-40-105 °C(GB/T 26149-2010)
Emission Power	-15-2dBm
Modulation Mode	ASK
Channel Bandwidth	300kHz
Data Rate	20kbps
PLL Lock Time	$<150\mu$s
PLL Phase Noise	-100dBc/Hz@300kHz
Power Consumption	$<$10mA

Part 15, we get 433MHz data transmitter design parameters in Tab.1.

III. THE 125 kHz WAKE-UP RECEIVER

In this section, we will introduce the architecture of the receiver and also derive the main design parameters to meet the wireless communication requirement analyzed in section II-A.

A. ARCHITECTURE OF THE WAKE-UP RECEIVER

Architecture of the proposed 125kHz wake-up receiver is shown in Fig.5. It consists of off-chip LC matching network, logarithmic amplifiers, full-wave rectifier (FWR), current summation unit, data filter, peak detector, hysteresis comparator and digital logic processing unit. The number of receiver channels has a great impact on reliability and power consumption of the TPMS. On one hand, the less channels, the less power consumption. On the other hand, the more channels, the higher reliability. If there is only one channel, the system will break down once this channel fails to process the received wake-up signals. Considering the receiver normally operates in monitoring mode and its power consumption, and to improve the communication reliability of the wake-up system in harsh electromagnetic environment, this design adopts dual channel structure with two orthogonal placed receiver antennas.

Logarithmic amplifier processes the contradiction among input dynamic range, power consumption and set-up time. After full-wave rectified, current signal is transformed into voltage signal by data filter, and the hysteresis comparator transforms the detected wake-up signal into logic high voltage. When the wake-up condition is satisfied, the receiver will output a wake-up signal to wake up the in-tire monitoring module.

The logarithmic amplifier is used to realize the dynamic range compression of the input detection signal; the full-wave rectifier is used to achieve ASK demodulation. The logarithmic amplifier adopts a multi-stage amplifier to amplify the detection signal step-by-step to approximate the logarithmic characteristic without requiring a single-stage amplifier with logarithmic transmission characteristics. The single-stage amplifier is actually a limiting amplifier, when the input amplitude is less than a certain threshold, the gain is constant; when the input amplitude is greater than the threshold, the gain is 0. Assuming that the input signal V_{in} gradually increases from 0, when the input signal V_{in} is relatively small, the Nth cascaded amplifier has not entered the saturation state, then the output V_{out} can be expressed as

$$V_{out} = AV_{in} + AV_{in}^2 + AV_{in}^3 + \cdots + AV_{in}^n \tag{17}$$

where, A is the gain when the single-stage amplifier is not saturated, and V_L is the amplitude of the output voltage when the single-stage amplifier enters the saturation state. When V_{in} is increased to V_k so that the kth stage just enters the clipping state, then we get

$$V_{in} = V_k = \frac{V_L}{A^{n-k+1}} \tag{18}$$

$$V_{out} = V_{ok} = kV_L + \frac{V_L}{A} + \frac{V_L}{A^2} + \cdots + \frac{V_L}{A^{n-k}}. \tag{19}$$

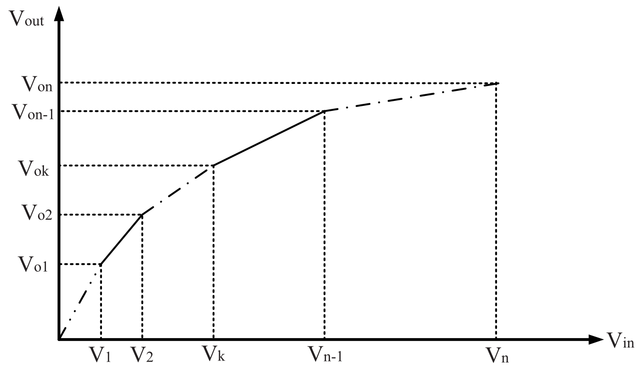

FIGURE 6. The voltage transmission characteristic curve of the logarithmic amplifier.

Combining Eq.(18) and Eq.(19), we have

$$k = \frac{1}{lnA} ln\left(\frac{V_{in}A^{n+1}}{V_L}\right) \tag{20}$$

$$V_{out} = V_{ok} = \frac{1}{lnA} ln\left(\frac{V_{in}A^{n+1}}{V_L}\right) V_L + \frac{V_L}{A} + \cdots + \frac{V_L}{A^{n-k}}. \tag{21}$$

Each of the points where the amplifier is saturated is marked in the figure and connected in a straight line to obtain the transmission characteristic curve of the logarithmic amplifier, as shown in Fig.6. The lower limit of the dynamic range is $V_{inmin} = V_L/A^n$. In order to obtain the logarithmic transmission relation, A should be large and $k > 0$, and at least the last stage enters the clipping state. The upper limit of the dynamic range of the logarithmic amplifier is the input amplitude $V_{inmax} = V_L/A$ when the first stage enters the clipping state. The input dynamic range is

$$D_{in} = V_{inmax}/V_{inmin} = A^{n-1}. \tag{22}$$

As can be seen from Eq.(22), dynamic range of the logarithmic amplifier is a function of the number of the logarithmic amplifier stages. Thus, it will increase by increasing the single-stage gain or stages. Accuracy of the logarithmic amplifier can be approximated as in

$$\delta_{max} = |y_2 - y_1|_{max}/y_1 \tag{23}$$

where y_2 is the polyline shown in Fig.6 and y_1 is the ideal logarithmic characteristic curve. When $A \gg 1$, y_1 is represented by Eq.(19), we can get

$$\delta_{max} \approx 1 - \frac{k + 1/lnA}{k + 3 - ln(lnA)/lnA} \tag{24}$$

$$\delta_{max} \approx 1 - \frac{klnA + 1}{klnA + ln(A^3/lnA)}. \tag{25}$$

From Eq.(23-25) we find, once the single-stage gain A fixed, the higher the number k, the higher the accuracy δ_{max}; Once the number of stages k is fixed, the higher the single-stage gain A, the lower the accuracy δ_{max}. The larger the single-stage gain A of the logarithmic amplifier, the larger the dynamic range and the lower the accuracy δ_{max}. The more the stages, the greater the dynamic range and the more increase of power consumption. Therefore, design of the logarithmic amplifiers is a compromise between dynamic range, stability, accuracy and power consumption.

The dynamic range is theoretically proportional to A^{n-1}. In practice, the lower limit of the dynamic range depends on the noise floor and receiver signal to noise ratio requirement. Actual signal transmission distance is about 20m. Considering the direction, disturbance and emission power of the wake-up transmitter, the required dynamic range is about 50dB. Combining the above analysis with the application of this design, the single-stage gain of the logarithmic amplifier is set to 14 dB and the number of stages is 5, thus the calculated dynamic range is 56dB, which meets the specification.

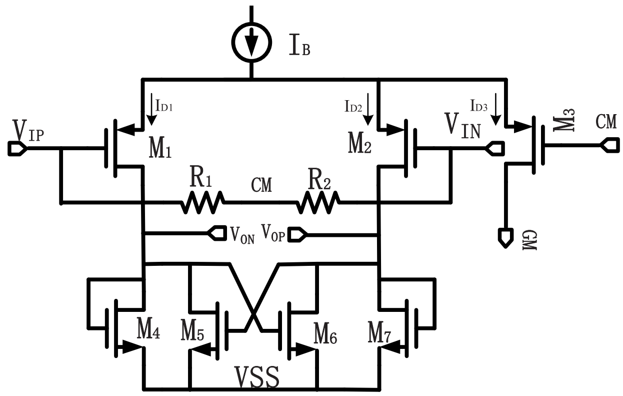

FIGURE 7. Schematic of logarithmic amplifier associated with full-wave rectifier.

B. DESIGN OF WAKE-UP RECEIVER CIRCUIT

1) LOGARITHMIC AMPLIFIER WITH FULL-WAVE RECTIFIER

Schematic of the single stage logarithmic amplifier associated with full-wave rectifier is shown in Fig.7. M_1, M_2 and M_3 have the same size; M_1 and M_2 form a differential amplifier, acting as the limiting amplifier. M_3 acts as the transconductance unit, its gate is connected to the gate of M_1 and M_2 through high value resistors R_1 and R_2; M_3 has the same common-mode voltage with M_1 and M_2. The output current of M_3 mainly consists of two parts, one is a constant current related to the common-mode bias voltage; the other is a varying current which has an approximate linear relationship with the input AC signal [17]. When there is no input signal, $I_{D1} = I_{D2} = I_{D3} \approx I_B/3$; When V_{IP} is very large, M_1 off, M_2 turns on, then $I_{D2} \approx I_B$, $I_{D1} = I_{D3} \approx 0$; when V_{IN} is very large, M_2 off, M_1 turns on, then $I_{D1} \approx I_B$, $I_{D2} = I_{D3} \approx 0$; when V_{IP} and V_{IN} are between 0 and very large value, I_{D3} is between $I_B/3$ and 0. The input voltage is converted to current signal, while its strength is approximate linear with the input voltage signal, which achieves full-wave rectification [17], [18]

$$I_B = I_{D1} + I_{D2} + I_{D3} \tag{26}$$

$$A = \frac{g_{m1}}{g_{m4} - g_{m5}} \tag{27}$$

$$g_{m,wi} = \frac{2I_{DS,wi}}{nkT/q}. \tag{28}$$

M3 operates in linear region, and the current is

$$\mathrm{I_{DS}} = \mathrm{u_n C_{ox}} \frac{\mathrm{W}}{\mathrm{L}} \left[(\mathrm{V_{GS}} - V_{\mathrm{TH}})\, \mathrm{V_{DS}} - \frac{1}{2} \mathrm{V_{DS}^2} \right] \tag{29}$$

When $\mathrm{V_{DS}}$ is small, Eq.(29) can be expressed as

$$\mathrm{I_{DS}} = \mathrm{u_n C_{ox}} \frac{\mathrm{W}}{\mathrm{L}} (\mathrm{V_{GS}} - \mathrm{V_{TH}})\, \mathrm{V_{DS}}. \tag{30}$$

2) HYSTERESIS COMPARATOR

Logarithmic amplifier's small signal gain is very high, so it is sensitive to noise and disturbance. Hysteresis comparator can reduce such interference, and it can also convert the ASK demodulated signal into digital one to the subsequent digital logic processing unit.

There are two feedback paths in Fig.8. The first is M_1 and M_2 common source node's serial current negative feedback [19]; the second is parallel voltage positive feedback which connecting M_5 and M_6's gate and drain [20].

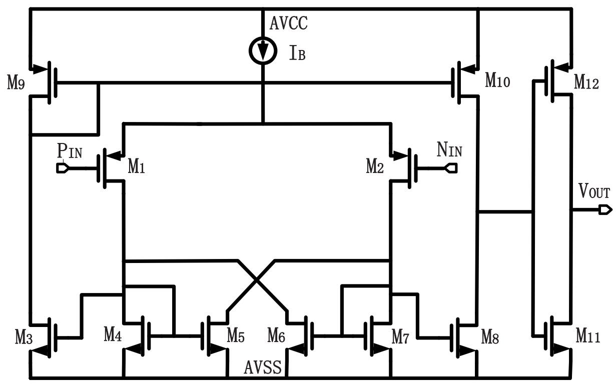

FIGURE 8. Schematic of hysteresis comparator.

When the positive feedback coefficient is smaller than the negative one, the circuit will show a negative feedback and lose hysteresis effect. While the positive feedback coefficient is bigger, the circuit will have positive feedback, and the voltage transfer curve has hysteresis effect. So it requires that the aspect ratio of M_5, M_6 is larger than that of M_4, M_7 in order to achieve positive feedback.

3) DIGITAL LOGIC PROCESSING CIRCUIT

After processed by the hysteresis comparator, the wake-up signal is sent to the digital logic processing unit. Schematic of the digital logic processing circuit is shown in Fig.9.

The wake-up signals are counted by the digital logic circuit, once they reach certain number, the receiver will output a wake-up signal. Then it wakes up the power management module or MCU, leading the in-tire monitoring SoC start to work. The wake-up signal will keep logic high until the receiver obtains a reset signal from the MCU, and then the receiver goes to next work cycle.

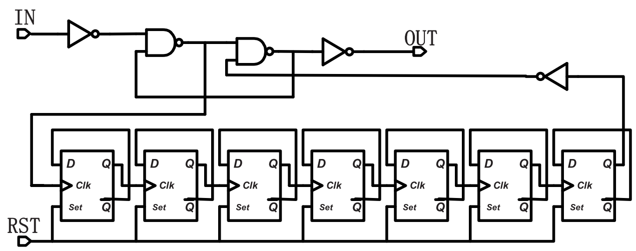

FIGURE 9. Schematic of the digital logic processing circuit.

C. WAKE-UP RECEIVER IMPLEMENTATION AND TEST

Based on the structure shown in Fig.5, the 125kHz wake-up receiver is fabricated in 0.35μm high voltage (HV) BCD process and draws no more than 5μA from a 3.3V power supply. Microphotograph of the 125kHz wake-up receiver, the evaluation board and the test environment are shown in Fig.10, Fig.11 and Fig.12, respectively. Total area and active area of the receiver are 1.4mm^2 and 0.48mm^2, respectively.

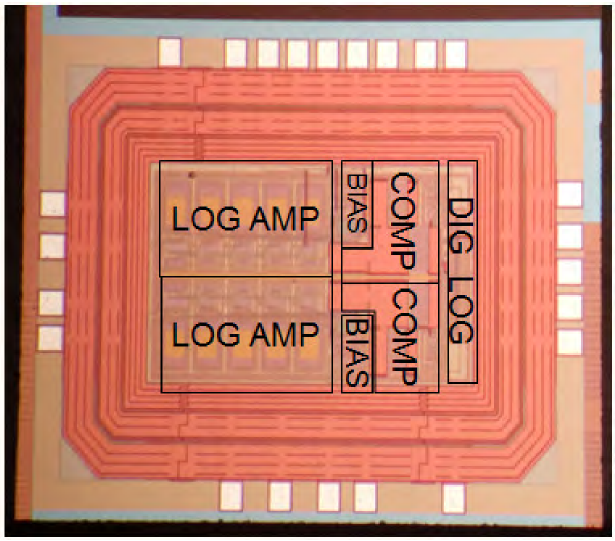

FIGURE 10. Chip microphotograph of wake-up receiver.

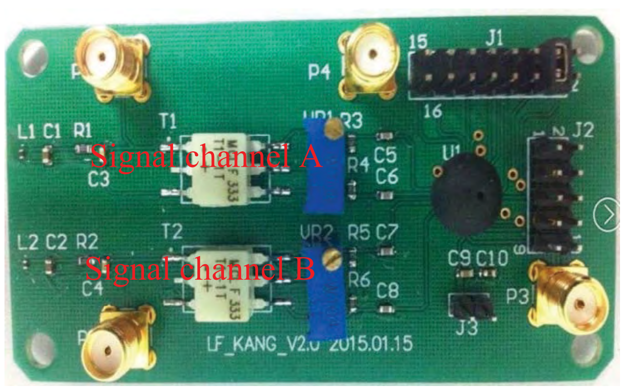

FIGURE 11. Evaluation board of wake-up receiver.

The ASK demodulation output and wake-up output of the receiver is shown in Fig.13. As can be seen, the receiver can

TABLE 2. 125 kHz low frequency wake-up receiver's test results compared with similar commercial products.

Parameter	This work	ATA5283 [21]	MCP2030 [22]	AS3932 [23]
Supply Voltage(V)	2.8V-5.5V	2-3.8V	2-3.6V	2.4-3.6V
Current	5μA(2 channel)	1μA	13μA (3 channel)	8.3-12μA(3 channel)
Temperature Range	-40-125 °C	125 °C (Max)	-40-85 °C	-40-85 °C
Sensitivity	0.5mVpp	1mVrms	3mVpp	100μVrms
Carrier Frequency	125kHz±20%	125kHz	125kHz	110-150kHz
Data Rate	35kbps(Max)	4kbps(Max)	10kbps(Max)	0.5-4kbps

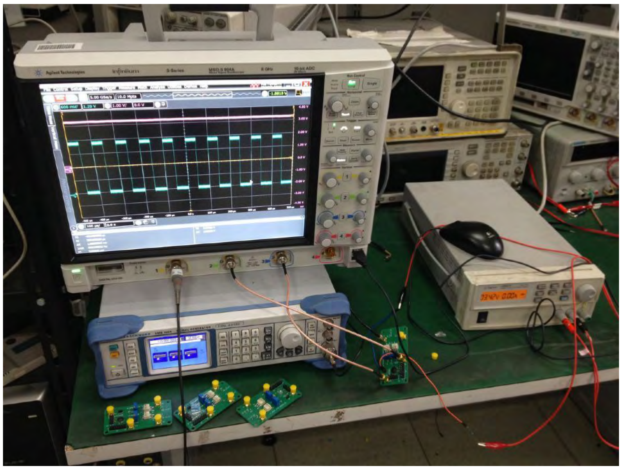

FIGURE 12. Test environment of the wake-up receiver.

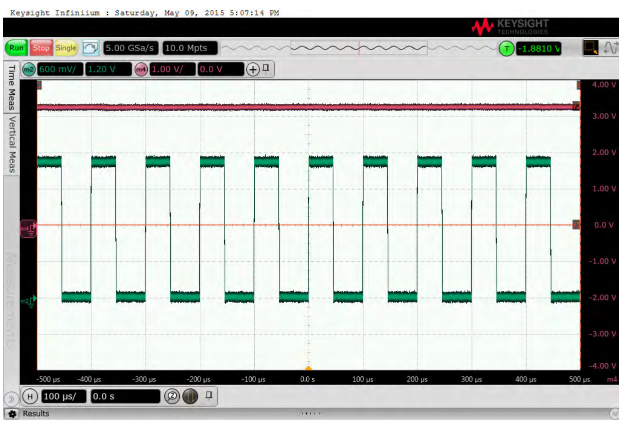

FIGURE 13. Wake-up receiver's ASK demodulation output and wake-up output.

demodulate ASK modulated wake-up signal correctly, when the wake-up condition is met, it will output a logic one signal to wake up the in-tire monitoring SoC.

Test results of the 125kHz wake-up receiver compared with similar commercial products are shown in TABLE.2.

IV. 433MHZ DATA TRANSMITTER

The data transmitter is composed of PLL, power amplifier (PA) and ASK modulator. In this section we will discuss the design process of the transmitter.

A. ARCHITECTURE OF THE 433MHZ DATA TRANSMITTER

Fig.14 shows the architecture of the proposed data transmitter. The on-chip part is in red dashed box, which consists of PLL (within the black dotted box), ASK modulator, power management unit and PA. The 433.92MHz carrier is generated by the integer N-type PLL. With the PLL providing carrier signal, MCU modulate the carrier signal through an ASK modulator. Then, the tire status data collected by the RSM module is transmitted to the central control module (CCM).

To reduce power consumption, this design adopts three power modes: data transmission mode, sleep mode and PLL mode. When data transfer is required, the transmitter works on data transmission mode, which of the maximum power consumption, both PLL and PA are working; When no data transfer, the transmitter works on sleep mode, which of the minimum power consumption, both PLL and PA are closed; When data transfer is required, but the PLL is not locked, the transmitter works on PLL mode; at this time, the PLL is working, but PA closed. The power consumption in this paper refers to data transmission mode.

B. THE DESIGN PROCESS OF PLL

As shown in Fig.15, the PLL is an integer N-type charge pump phase-locked loop; through the frequency discriminator's frequency monitoring function to increase the lock speed of the PLL; the PLL frequency range is approximately equal to the frequency tuning range of the VCO. The PLL is composed of frequency discriminator/charge pump (PFD/CP), loop filter (LPF), voltage controlled oscillator (VCO) and frequency divider (DIV).

The working principle of the PLL is that the reference frequency provided by the external crystal (F_{xtal}) is input to the PFD/CP; PFD/CP performs frequency detection and amplifies the frequency error (ferr), and converts the phase error into a current proportional to the phase error amplitude; The current is converted to the corresponding value of the voltage through the LPF to control the VCO oscillation frequency; The DIV divides the output of the VCO by negative feedback to the PFD, and reduces the ferr of the PFD, simultaneously. When ferr is small enough, the phase detector (PD) starts to work and the phase discrimination process is similar to the above-mentioned frequency discrimination process.

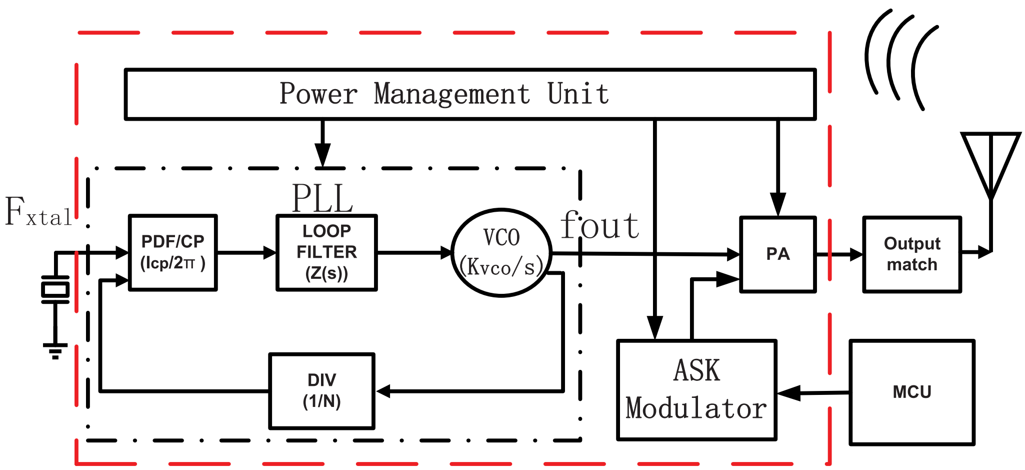

FIGURE 14. The architecture of 433MHz data transmitter.

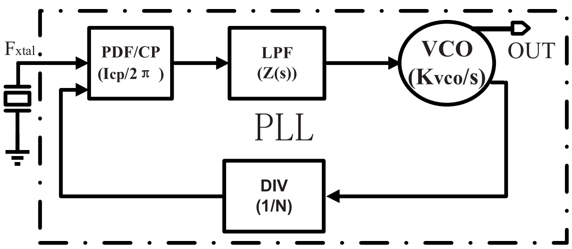

FIGURE 15. Structure of the PLL for 433MHz data transmitters.

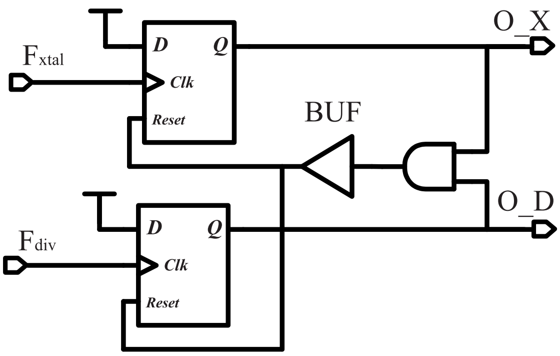

FIGURE 16. Schematic of the PFD.

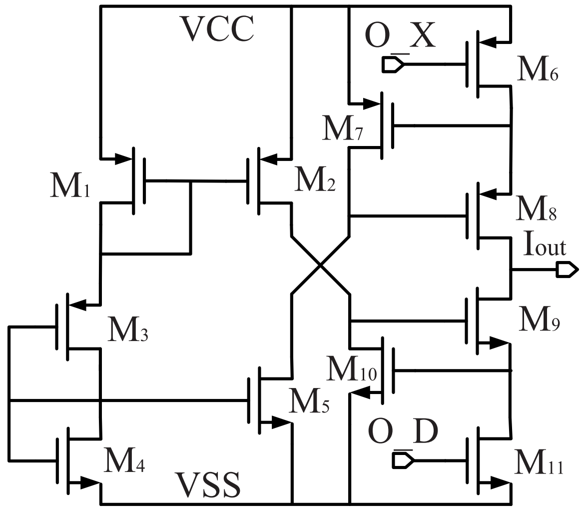

FIGURE 17. Schematic of the charge pump.

1) PHASE AND FREQUENCY DETECTOR

Schematic of the PFD is shown in Fig.16. If $F_{div} < F_{xtal}$, O_X will be a series of pulses, and O_D remains 0. If opposite, O_X will keep as 0, and O_D outputs pulses, thereby completing frequency detecting function. If F_{div} and F_{xtal} are the same frequency, but the F_{div}'s phase is behind F_{xtal}'s, O_X will be a series of pulses, with pulse width proportional to the phase difference between F_{xtal} and F_{div}, and O_D remains 0. Similarly, in the opposite condition, O_X will be 0, and O_D is a series of pulses. Thus, the phase detecting function is fulfilled.

The presence of O_X and O_D's rising and falling delay will lead to dead time effect (pulse width is not proportional to the phase difference). By adding a buffer (Buf) to delay the narrow pulse while O_X and O_D is high, this effect can be weakened.

2) CHARGE PUMP

Schematic of the charge pump is shown in Fig.17. When O_X is logic low and O_D is logic high, M_6 and M_{11} turn on, simultaneously (state before charge pump reset). And when O_X is logic high, and O_D is logic low, M_6 and M_{11} turn off, so the charge pump neither draws current from I_{OUT} nor injects current to I_{OUT}. When O_X and O_D are both logic low, M_6 is on, M_{11} is off, the charge pump injects current to I_{OUT} through M_6 and M_8. When O_X and O_D are both logic high, M_6 turns off, and M_{11} turns on, the charge pump draws current from I_{OUT} via M_9 and M_{11}.

Additional attention should be paid on the current match when designing charge pump. If the match is poor, there

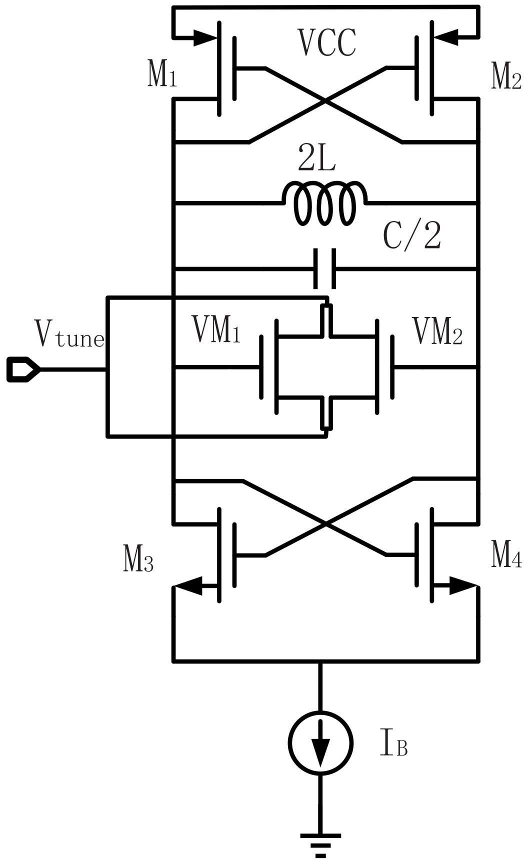

FIGURE 18. Schematic of the negative resistance structure LC VCO.

will be cyclical fluctuations on the VCO control voltage after PLL lock. These cyclical fluctuations will worsen PLL's frequency stability and phase noise performance. M_6, M_8 and M_9, M_{11} are cascoded to increase the output impedance and reduce current mismatch at the same time.

3) VOLTAGE CONTROLLED OSCILLATOR

Schematic of the negative resistance LC VCO is shown in Fig.18. PMOS transistor M_1 and M_2, along with NMOS transistors M_3 and M_4 consist two cross-coupled structures to provide negative resistance; PMOS and NMOS cross-coupled structures can provide higher transconductance to enhance the switching speed of the MOS switch; this structure can also achieve the benefit of improved phase noise performance caused by symmetry properties simultaneously.

VCO operates in current restricted zone to reduce its impact on the supply voltage. Capacitance C is used to adjust the VCO's voltage sensitivity Kvco. If Kvco is much too high, it will cause the deterioration of the PLL's phase noise performance; but if Kvco is much too low, the frequency tuning range of the VCO will be restricted and thus affects the lock up of PLL. So the value of C should be carefully chosen to get best performance [24].

Since China has no short-range wireless communication standard, for convenience, this design refers the

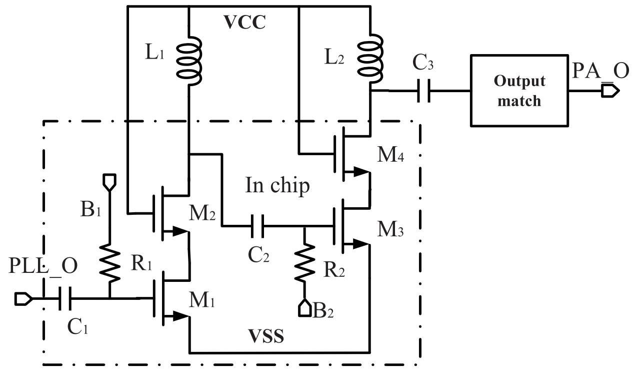

FIGURE 19. Schematic of the class AB PA.

similar European standard to derivate the PLL's phase noise request [15]

$$PN < Pr_{\min} - Pi_{\max} - BWc - SNR \tag{31}$$

wherein PN is the phase noise; $Pr_{\min}$ is the minimum received signal power; $Pi_{\max}$ is the maximum power of interference signal; BWc is channel bandwidth. The minimum received power can be expressed as

$$Pr_{\min} = \frac{10}{16} \lg BW - 107(\mathrm{dBm}) = -64.26(\mathrm{dBm}). \tag{32}$$

Considering the design margin, the minimum received power is set to −80dBm. When the short-range wireless communication system receiver blocking characteristic requirements are considered, the phase noise with 300kHz carrier frequency offset is as follows:

$$PN@300KHz < -99.7\mathrm{dBc/Hz}. \tag{33}$$

C. THE CLASS AB POWER AMPLIFIER (PA)

Schematic of the class AB PA is shown in Fig.19. The core function module of the PA (in dashed box) is integrated; M_1, M_2, M_3 and M_4 are RF NMOS transistors. L_1 and L_2 act as choke inductors, and they can only be achieved by off-chip because of their large values.

Since the values of the capacitance and inductance in the matching network are relatively large, the output matching network is also implemented off-chip. Since it is very difficult for single-stage PA to achieve a 15-20dB power gain, this design adopts a two-stage structure, which are the pre-driver stage and the power output stage.

M_1 and M_2 are cascoded to provide higher gain to increase the isolation between the input stage and the subsequent power output stage, while providing a relatively high voltage swing. The power output stage that M3 and M4 constituted is designed to match the load line, and the sizes of M_3 and M_4 are determined by the conduction angle of the PA. B_1 and B_2 are bias voltage to ensure all the RF MOSs have right bias voltage. R1 and R2 are high-value resistors to ensure the accuracy of B_1 and B_2. The output matching network adopts quality factor controllable π matching network.

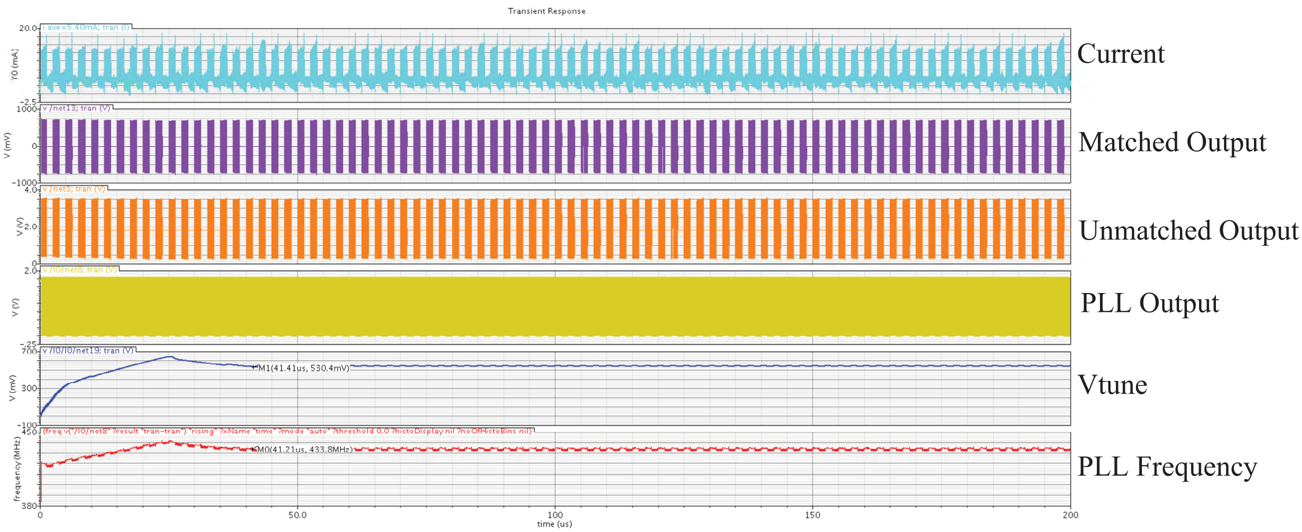

FIGURE 20. Post-layout simulation results of the data transmitter's ASK modulation.

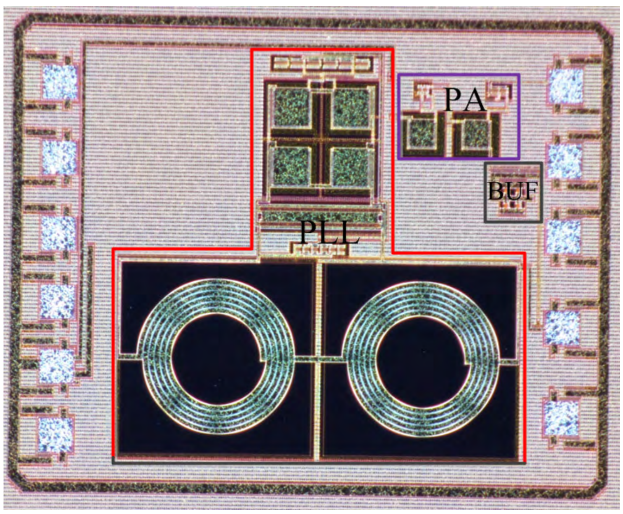

FIGURE 21. Chip microphotograph of the data transmitter.

Post-layout simulation results of the data transmitter's ASK modulation is shown in Fig.20. As can be seen, the PLL locked at 433.9MHz at 43μs.

D. DATA TRANSMITTER IMPLEMENTATION AND TEST

Based on the structure shown in Fig.14, the proposed 433MHz data transmitter is fabricated in the 0.18μm process and draws no more than 7.3mA from a 1.8V power supply. The microphotograph of the 433MHz data transmitter is shown in Fig.21. Total area of the data transmitter is 0.964 mm^2, and the active area is 0.64 mm^2.

As can be seen from Fig.22, the phase noise at 300kHz (channel bandwidth) is -102.93dBc/Hz, and this value can meet the TPMS's application requirement calculated in Eq.(33).

As seen from Fig.23, output power of the transmitter is -10.12dBm@433.92MHz. As this design adopts ASK modulation, thus, there are two sidebands, and the sidebands of output spectrum meet the specification.

Fig.24 shows that the data transmitter can transfer the data processed by MCU with ASK modulation in the form of electromagnetic waves to the 433MHz data receiver through an antenna.

Test results of 433MHz data transmitter and similar design are compared in TABLE.3.

TABLE 3. Test results of 433MHz data transmitter and similar design.

Parameter	This Work	[25]	TDK5100 [26]
Supply Voltage	1.6-2V	1.6-2V	2.1-4V
Emission Power	-10dBm	3dBm	5-6dBm
Modulate Mode	ASK	ASK	ASK/FSK
Data Rate	30kbps	30kbps	20kbps
Power	13.14mW	25mW	27mW

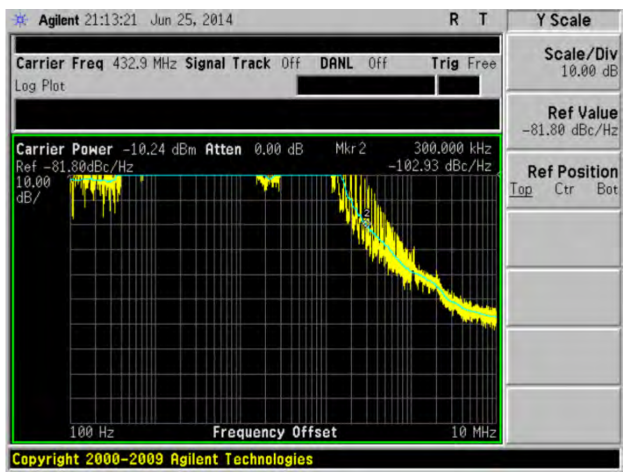

FIGURE 22. Phase noise of the data transmitter.

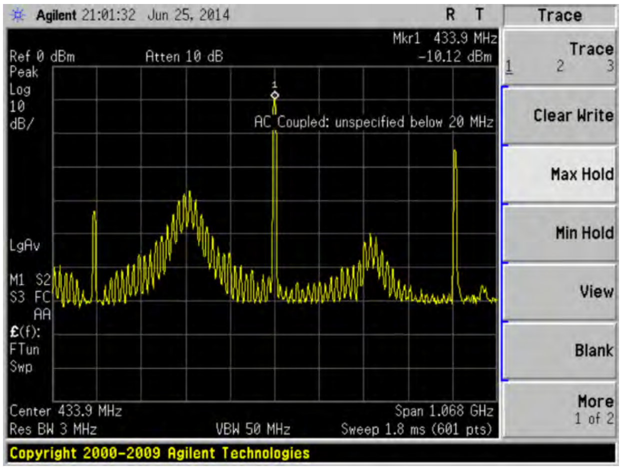

FIGURE 23. **Output spectrum of the data transmitter.**

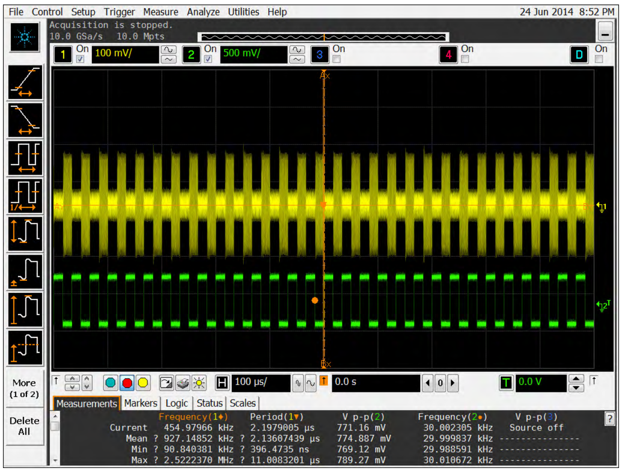

FIGURE 24. **Data transmitter's ASK modulated output.**

V. CONCLUSION

In order to eliminate the defect of the existing battery TPMS in the battery replacement and system performance affected by the battery status, we proposed the battery-less TPMS. Among them, the wireless energy transmission and energy receiving module has been able to normally drive the system based on commercial chips.

This paper mainly focuses on the in-tire wireless communication module of the battery-less TPMS, that is, the 125kHz wake-up receiver and the 433MHz data transmitter.

According to the TPMS application requirements and the relevant wireless communication theory, the design parameters of the two modules are described in detail. On the basis of theoretical calculation, the principle and design of each circuit module of LF wake-up receiver and data transmitter are derived in detail, and the related chip is fabricated and tested.

Based on 0.35μm CMOS HV BCD process, the 125kHz wake-up receiver is designed and taped out. With low noise, low mismatch and sub-threshold design, and the logarithmic amplifier to achieve ASK demodulation and dynamic range compression, the power consumption of the receiver is very low.

Test results show that the operating voltage range is 2.8-5.5V, with the overall work current of 5μA under 3.3V supply voltage, operating temperature range of -40-125 °C, sensitivity of 0.5mVpp, carrier frequency ranges of 125kHz$\pm$ 20%, and the data rate of 35kbps (Max). The overall performance meets the TPMS application requirements.

The 433MHz data transmitter is designed in 0.18μm process and taped out. Test results show that the operating voltage range is 1.6-2.0V, with frequency tuning range of 410-450MHz, and transmit power of -10dBm@433.92MHz, PLL phase noise of -103dBc/Hz@300kHz, and typical operating current of 7.3mA under 1.8V supply voltage. All the parameters meet the application requirements.

With commercial 433MHz data receiver and 125kHz data transmitter, the designed chips and commercial chips realize wireless communication of battery-less TPMS. We test the wake-up communication link and data transmission link in system level. System-level test results show that the design of the tire wireless communication module can work well in 20m, which meets most vehicle requests; and the wireless communication program is feasible. Our future research work will focus on the processing of tire status data.

ACKNOWLEDGMENT

We give thanks for the insightful discussion and help of Hanjun Jiang, Liji Wu, Xiangmin Zhang from Institute of Microelectronics, and Quanyong Xu from School of Aerospace Engineering, Tsinghua University.

Finally, we give great thanks to the anonymous reviewers for their suggestions to improve the quality of this paper.

REFERENCES

[1] *Tire Pressure Monitoring System*, Standard, N.H.T.S. Admin., 2005.

[2] *Tire Pressure Monitoring Systems for Light Duty Highway Vehicle*, Standard 2004-12, S.o.A. Engineers.

[3] *Road Vehicles-Safety Enhancement in Conjunction With Tyre Inflation Pressure Monitoring*, Standard 2006-03-15, I.-E. ISO, I.O.f.S.

[4] *TPM Sensor Module Based Tire Pressure Monitoring Systems for Motor Vehicles*, Standard, G. SAC, S.A.o.C., 2010.

[5] Y. Li, L. Wu, C. Zhang, and Z. Wang, "Power recovery circuit for battery-less TPMS," in *Proc. 7th Int. Conf. ASIC (ASICON)*, Oct. 2007, pp. 454–457.

[6] L. Chen, A. G. Helmy, G. Yue, S. Li, and N. Al-Dhahir, "Performance analysis and compensation of joint TX/RX I/Q imbalance in differential STBC-OFDM," *IEEE Trans. Veh. Technol.*, vol. 66, no. 7, pp. 6184–6200, Jul. 2017.

[7] P. Papazian, "Basic transmission loss and delay spread measurements for frequencies between 430 and 5750 MHz," *IEEE Trans. Antennas Propag.*, vol. 53, no. 2, pp. 694–701, Feb. 2005.

[8] S. Vellucci, A. Monti, M. Barbuto, A. Toscano, and F. Bilotti, "Use of mantle cloaks to increase reliability of satellite-to-ground communication link," *IEEE J. Multiscale Multiphys. Comput. Techn.*, vol. 2, pp. 168–173, 2017.

[9] S. Wu, L. Kuang, Z. Ni, D. Huang, Q. Guo, and J. Lu, "Message-passing receiver for joint channel estimation and decoding in 3D massive MIMO-OFDM systems," *IEEE Trans. Wireless Commun.*, vol. 15, no. 12, pp. 8122–8138, Dec. 2016.

[10] Y. Okumura, E. Ohmori, T. Kawano, and K. Fukuda, "Field strength and its variability in VHF and UHF land-mobile radio service," *Rev. Elect. Commun. Lab*, vol. 16, nos. 9–10, pp. 825–873, 1968.

[11] K. A. Chamberlin and R. J. Luebbers, "An evaluation of Longley-Rice and GTD propagation models," *IEEE Trans. Antennas Propag.*, vol. AP-30, no. 6, pp. 1093–1098, Nov. 1982.
[12] A. Goldsmith, *Wireless Communications*. Cambridge, U.K.: Cambridge Univ. Press, 2005.
[13] J. D. Griffin, G. D. Durgin, A. Haldi, and B. Kippelen, "RF tag antenna performance on various materials using radio link budgets," *IEEE Antennas Wireless Propag. Lett.*, vol. 5, pp. 247–250, 2006.
[14] H. W. Huang, K. H. Chen, and S. Y. Kuo, "Dithering skip modulation, width and dead time controllers in highly efficient DC-DC converters for system-on-chip applications," *IEEE J. Solid-State Circuits*, vol. 42, no. 11, pp. 2451–2465, Nov. 2007.
[15] *Electromagnetic Compatibility and Radio Spectrum Matters (ERM)*, document ETSI EN 300 220-1 V2.3.1, Short Range Devices (SRD).
[16] *Part 15-Radio Frequency Devices; 15.231 Periodic Operation in the Band 40.66–40.70 MHz and Above 70 MHz*, document, F. C. Commission, 2011.
[17] C. D. Holdenried, J. W. Haslett, J. G. McRory, R. D. Beards, and A. J. Bergsma, "A DC-4-GHz true logarithmic amplifier: Theory and implementation," *IEEE J. Solid-State Circuits*, vol. 37, no. 10, pp. 1290–1299, Oct. 2002.
[18] P. A. K. Moon, "Signal strength detector," U.S. Patent 4 620 114, Oct. 28, 1986.
[19] M. Jacob and C. C. Halkias, *Integrated Electronics: Analog and Digital Circuits and Systems*. 1972.
[20] P. E. Allen and D. R. Holberg, *CMOS Analog Circuit Design*. London, U.K.: Oxford Univ. Press, 2002.
[21] *Interface IC for 125 KHz wake-Up Function ATA5283 Preliminary*, Atmel, San Jose, CA, USA.
[22] *Three-Channel Analog Front-End Device MCP2030*, Microchip, Chandler, AZ, USA.
[23] *As3932 3D Low Frequency Wakeup Receiver Revision 1.2*, Austriamicrosystems, Unterpremstätten, Austria, 2009,
[24] A. Hajimiri and T. H. Lee, "Design issues in CMOS differential LC oscillators," *IEEE J. Solid-State Circuits*, vol. 34, no. 5, pp. 717–724, May 1999.
[25] J. Zhu, L. Wu, X. Zhang, C. Jia, and C. Zhang, "A low-power 433 MHz transmitter for battery-less tire pressure monitoring system," in *Proc. IEEE 9th Int. Conf. ASIC (ASICON)*, Oct. 2011, pp. 184–187.
[26] *Wireless components ASK/FSK Tranzsmitter868/433 MHz, TDK 5100 Version 1.1*, i Technologies, May 2012.

QINMIAO KANG was born in Xuchang, China, in 1987. He received the B.S. degree from the Tianjin University of Technology in 2012 and the M.S. degree from the University of Tsinghua University. He is currently pursuing the Ph.D. degree with the School of Aerospace Engineering, Tsinghua University, Beijing, China.

His research interests include wireless communication network, wireless transmitter and receiver design, analog integrated circuit design, heavy oil helicopter control and diesel engine control.

XUDONG HUANG was born in Xining, Qinghai, China, in 1981. He received the B.Eng. and Ph.D. degrees from Tsinghua University in 2004 and 2010, respectively. He finished his post-doctoral research in 2012 and is currently an Assistant Professor with the School of Aerospace Engineering, Tsinghua University.

His research interests include aero-engine control, turbomachinery, and CFD.

YONG LI (M'09–SM'16) received the B.S. degree in electronics and information engineering from the Huazhong University of Science and Technology, Wuhan, China, in 2007, and the Ph.D. degree in electronic engineering from Tsinghua University, Beijing, China, in 2012. He is currently a Faculty Member with the Department of Electronic Engineering, Tsinghua University.

He has served as the general chair, the TPC chair, and a TPC member for several international workshops and conferences. He is on the editorial board of three international journals. His papers have total citations over 2300 (six papers exceed 100 citations and Google Scholar). Among them, eight are ESI Highly Cited Papers in Computer Science, and four receive conference best paper (run-up) awards. He received the IEEE 2016 ComSoc Asia–Pacific Outstanding Young Researchers and Young Talent Program of China Association for Science and Technology.

ZHIFENG XIE was born in Yili, China, in 1982. He received the M.S. degree from Zhejiang University in 2005 and the Ph.D. degree in theoretical physics from the Chinese Academy of Sciences in 2010. Since 2010, he was a Research Assistant with the School of Aerospace Engineering, Tsinghua University, Beijing, China. His research interests mainly include the design of aeroengine, structural dynamics, fluid mechanism, vibration control, and engine electronic control.

YONGQUAN LIU was born in 1963. He received the B.S. degree in aeroengine design from Northwestern Polytechnical University in 1984, the M.S. and Ph.D. degrees from Beihang University. He is currently a Researcher and Doctoral Tutor with the 606 Institute, Chinese Aeronautical Establishment.

His research interests include: Turbine engine design, rotor dynamics, advanced technology and informatization of aircraft engines, overall design and planning of aeroengine, structural strength and vibration, mechanical dynamics, and machine vibration diagnosis and control.

MING ZHOU was born in 1962. He received the B.S. degree from Northwestern Polytechnical University in 1984, and the M.S. and Ph.D. degrees from Beihang University in 1993 and 1996, respectively, and the Ph.D. degree in power engineering and control from Tsinghua University.

He is currently a Professor with the School of Aerospace Engineering, Tsinghua University, Beijing, China. His research interests include diesel engine design, engine control, rotor-bearings dynamics, and fuel injection system design.